IEEE Transaction on Industrial Electronics, Vol. 58, Iss. 1 , pp. 85-94, Jan. 2011, TIE-09-1370

Power Control Design of a battery charger in a Hybrid Active PV generator for load-following applications

Hicham Fakham, Di Lu, Bruno Francois, *Senior Member, IEEE*

***Abstract*— A hybrid generator with a PV energy conversion system is proposed with supercapacitors and lead-acid batteries in a DC-coupled structure. The objective of this system is to supply prescribed reactive and active power to the grid. This presented work focuses on the strategy, which makes it possible to ensure a high battery state of charge and an overcharge security by designing a dedicated local control system. A continuous dynamic model and a control design of the power system studied are proposed in this paper. Simulation and experimental results illustrate the performances obtained.**

***Index Terms*— Hybrid power system, PV generator, distributed generator, power control, energy management.**

I. Introduction

Currently Photovoltaic (PV) generators are designed in order to generate a maximum power to the grid. Because of the stochastic nature of the PV power output, large developments of grid-connected PV systems involve large fluctuations of the frequency, power and voltage in the grid. Since some countries have adopted feed-in tariffs for grid-connected PV systems, such problems are now critical and the control of energy quality becomes more important than before.

Active Distributed Generators (DGs) have the potential to provide ancillary services under these circumstances. For example, they may have several functions as frequency control, instantaneous reserve, emergency supply, peak shaving, … To provide these grid services, the real and reactive grid power produced from PV generators have to be controlled [1], [2]. Hence, storage units (batteries, supercapacitors,…) or/and other energy sources (wind generator, diesel units,…) can be used to compensate the lack of power or to store the excess power [3], [4]. A coordinated use of storage units must be designed within the available renewable resource in order to satisfy the power requirements.

As shown in Fig. 1.a, the structure that has been widely used is based on the direct connection of a battery bank to the dc-bus of the grid-connected inverter [6]. A PV controller is used to extract the Maximum Power from PV panels and send it to the battery bank. However, the stochastic nature of the PV power output and power demand leads to a fast charge/discharge action of batteries and a fast battery ageing.

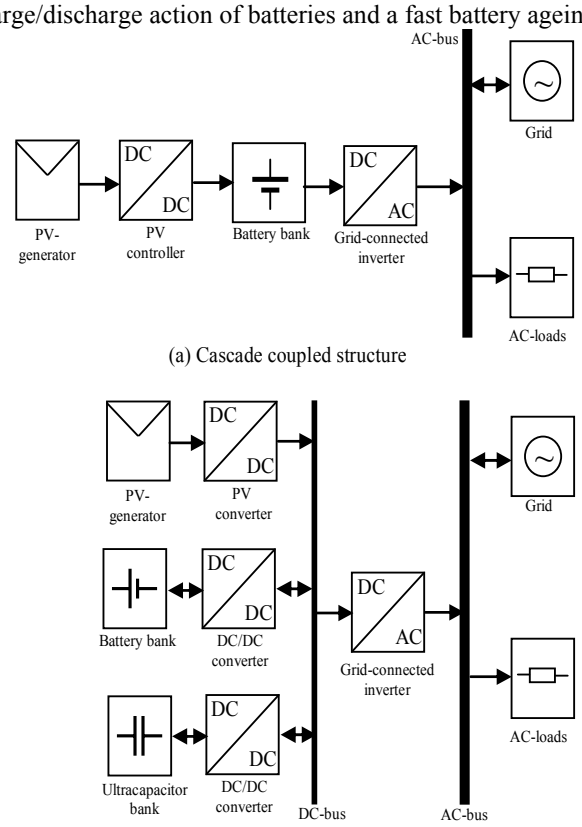

Fig. 1. Different schemes for hybrid PV generators including storage units.

To enable a more efficient use of batteries, a DC coupled structure has been presented in [7]. A first interest is that the battery bank is connected to the dc-bus via a DC/DC converter and, so makes it possible to obtain an optimised charge/discharge operation mode (see Fig. 1.b) [8]. A second advantage is that a super capacitor bank is added and is also connected to the dc-bus via another DC/DC converter. Batteries must be used for the long term supply of energy. Supercapacitors leads to a fast dynamic regulation of powers [9], [10]. The PV array is connected to the dc-bus via a PV converter. A power management and control method for this

Manuscript received July 30, 2009. This work was supported in part by the french Research National Agency: ANR project SUPERENER.

H. Fakham, D. Lu, B. Francois are with Univ Lille Nord de France, F-59000 Lille, France and with ECLille, L2EP F-59650 Villeneuve d'Ascq (e-mail: bruno.francois@ec-lille.fr).

Color versions of one or more of the figures in this paper are available online at http://ieeexplore.ieee.org

grid-connected PV generator including both storage units has to be designed in order to provide the real grid power reference required. One of the most important factors for the studied PV based DG are how efficiently:

- it can convert primary PV power into electricity;
- it can extract stored energy from batteries if the PV power is insufficient;
- it can store energy into batteries if the PV power is abundant.

The control strategy published in [11] considers the power management of batteries as a smoothing system. Hence, the overall system value can be greatly increased for the grid operator because this generator is then able to provide prescribed reactive and real powers. But a smoothing charge/discharge is insufficient to make an optimized battery storage operation possible (with a minimized cost) because the battery lifetime is limited and depends upon a number of operation factors (overcharge, charge level, temperature…). Another additional sophisticated control strategy for the battery charger is required to ensure a high battery SOC and an overcharge security, as well as increasing the battery lifetime. The innovation in this paper is to propose an accurate battery control strategy into the control system of this hybrid active PV generator.

Different charging methods for batteries have been proposed, but the charging principle is always the same. Charge controllers prevent an excessive battery from overcharging by interrupting or limiting the current flow from the solar array to the battery when the battery is fully charged. A battery-charging strategy, which has been widely applied in PV systems, is based on connecting or disconnecting directly the solar array to the battery bank [12]-[14]. The charging regulation is often performed when a prescribed cut-off voltage (gassing voltage or floating voltage) is reached. Consequently, only the first 70% to 80% of battery capacity is reached. In order to achieve the full capacity without causing overcharge, an alternative charging method based on on/off control is proposed in [15]-[17]. However, during the off-time no energy is transferred to the battery. Consequently, the available renewable energy is badly used and managed.

Another method proposes a battery-charging algorithm based on the state of charge (SOC) estimation [18], [19]. However, the accurate estimation of the SOC remains very complex and is difficult to be implemented. In order to avoid this complexity, specific regulation algorithms have been proposed: Maximum Power Point Tracking (MPPT) [20], fuzzy logic-based method [21]. However, these regulation algorithms can not operate with a grid-connected inverter and grid power references from a grid operator.

In this paper, the control system is detailed in Section II within the particular power management of the various units: PV, batteries, and supercapacitors. In Section III, the strategy of battery current tracking is developed in order to charge batteries at the high battery SOC levels, with a short time period and with overcharge security. A continuous dynamic model of lead-acid batteries charge voltage is exposed and then the control design proposed is detailed. To show the performances obtained, simulation results are presented, highlighting the long term evolution of electrical quantities in the batteries in the Section IV. In Section V, the grid service concerning the forced load-following requirement is recalled and experimental results are presented to demonstrate the real time power compensation of the supercapacitors and assess the good operation of the whole generator. Finally, some conclusions are given about the overall design.

II. CONTROL SYSTEM SCHEME

A. Organization

The control system is composed of three levels (see Fig. 2). Each one has precise control tasks depending on its hierarchical position [21]. The Switching Control Unit (SCU) provides the semiconductor signals ({-5, +15}) in order to apply the ideal states ({0, 1}) desired. A hybrid generator has four power converters and thus four SCU are used for each converter, as well as four Automatic Control Units (ACU). An ACU applies control algorithms to satisfy the current or voltage references. The Power Control Unit (PCU) calculates the power reference for each source according to the power balancing strategy.

B. Control of fast dynamic quantities

Control functions of fast dynamic electrical quantities have been detailed in [7], [11]. In order to get a constant DC bus voltage, a closed loop control of this voltage (see Fig. 2) sets the capacitor current (i_{dc_ref}) required.

The PV voltage (u_{pv}) is controlled to set the maximum PV power reference (p_{pv_ref}), which is calculated by a MPPT algorithm according to the "Power algorithms" level [23]. Current controllers are used to control the choke current (i_L), the grid currents (i_s), the supercapacitor current (i_{sc}) and the battery current (i_b). Calculated signals, $u_{m\_pv\_ref}$, $u_{m\_bat\_ref}$, $u_{m\_sc\_ref}$, $u_{m\_inv\_ref}$ obtained are the references wished, in mean values, of output voltages for, respectively the PV DC/DC converter, the battery DC/DC converter, the supercapacitor DC/DC converter and the inverter. The battery current reference is deduced by using the current tracking for a prescribed and optimized power with the battery. It will be detailed in Section III.

C. Power control

Current references for closed loop controls are found using inverse modelling equations R1 and R2, respectively for the supercapacitors and the PV (see Table 1).

By using a synchronized Park frame along with the grid voltages, the grid real power can be expressed with Park components of the grid voltages (v_{s_d}, v_{s_q}) and currents (i_{s_d}, i_{s_q}) (see Table I (R3)). By inverting these equations, the real power supply to the grid (p_{g_ref}) is regulated by setting the filter current references with a reactive power reference (see Table I (R3c)).

The required power for the DC bus regulation (p_{dc_ref}) and battery power (p_{bat_ref}) are calculated using the corresponding modelling equations (see Table I (R4e), (R5e)). The PV power available is estimated in a similar way (see Table I (R2e)).

D.Power algorithms

The 'power algorithms' level (see Fig. 2) comprises the MPPT algorithm [12], the power balancing algorithm (see Fig. 4) and the battery current tracking algorithm (see Fig. 7).

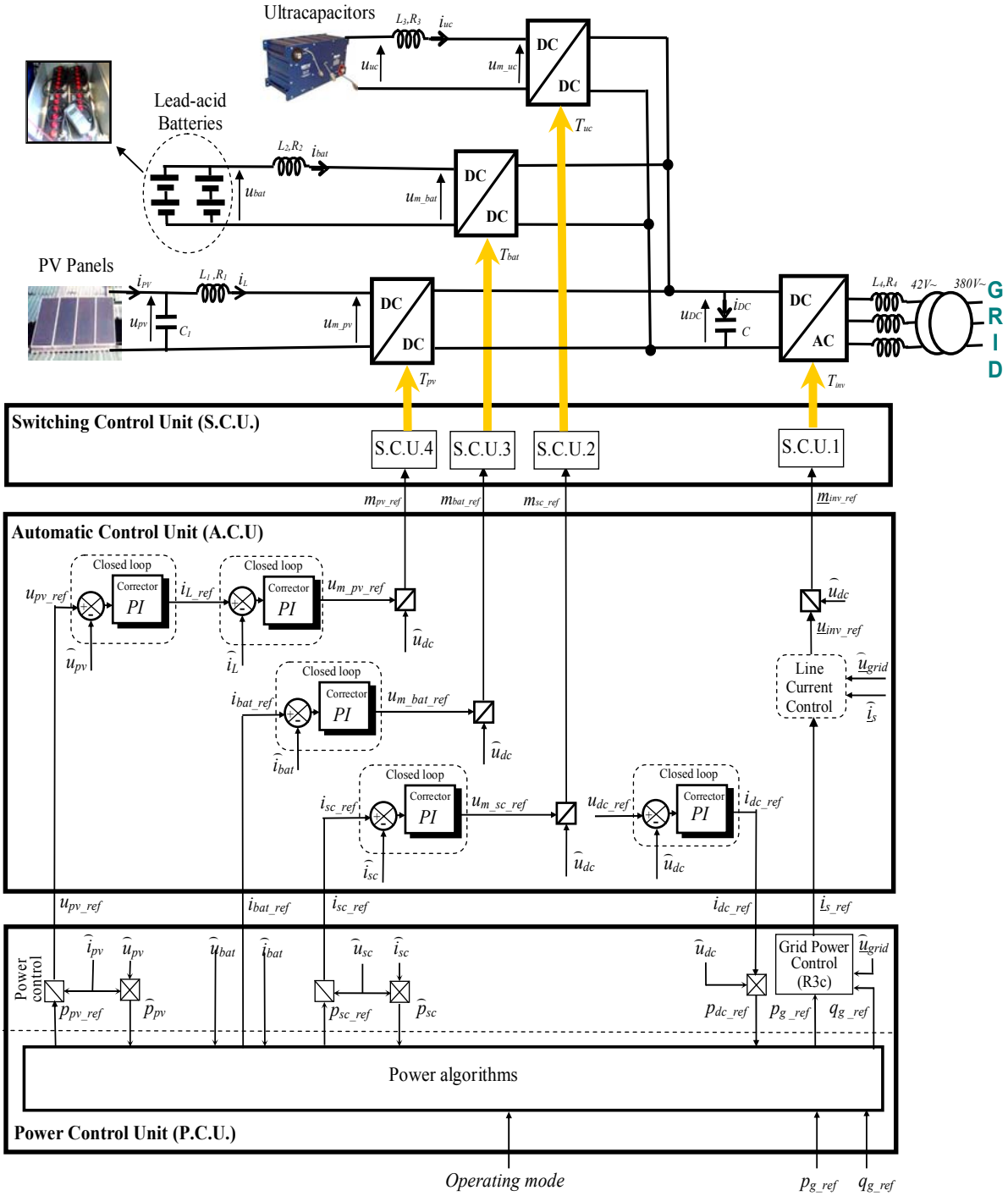

Fig. 2. Grid-connected Photovoltaic power system including batteries.

The MPPT algorithm used is a classical one and will not be detailed in this paper. The battery current tracking algorithm will be presented in Section III.

Storage units are used to implement the inner power balancing; the corresponding algorithm is now detailed.

TABLE I.
POWER MODELING AND CONTROL EQUATIONS

Modeling equations		Control equations	
$p_{sc} = u_{sc} i_{sc}$	(R1)	$i_{sc\_ref} = \frac{p_{sc\_ref}}{\hat{u}_{sc}}$	(R1c)
$p_{pv} = u_{pv} i_{pv}$	(R2)	$i_{pv\_ref} = \frac{p_{pv\_ref}}{\hat{u}_{pv}}$	(R2c)
		$\tilde{p}_{pv} = \hat{u}_{pv} \hat{i}_{pv}$	(R2e)
$\begin{cases} p_g = v_{s_d} i_{s_d} + v_{s_q} i_{s_q} \\ q_g = v_{s_d} i_{s_q} - v_{s_q} i_{s_d} \end{cases}$	(R3)	$\begin{cases} i_{s_{d\_ref}} = \frac{p_{g\_ref} \hat{v}_{s_d} - q_{g\_ref} \hat{v}_{s_q}}{\hat{v}_{sd}^{\,2} + \hat{v}_{sq}^{\,2}} \\ i_{s_{q\_ref}} = \frac{p_{g\_ref} \hat{v}_{s_q} + q_{g\_ref} \hat{v}_{s_d}}{\hat{v}_{s_d}^{\,2} + \hat{v}_{s_q}^{\,2}} \end{cases}$	(R3c)
$p_{DC} = u_{dc} i_{dc}$	(R4)	$p_{DC\_ref} = \hat{u}_{dc} i_{dc\_ref}$	(R4e)
$p_{bat} = u_{bat} i_{bat}$	(R5)	$p_{bat\_ref} = \hat{u}_{bat} i_{bat\_ref}$	(R5e)
$L_{filter} = R_s \left(i_{sd}^2 + i_{sq}^2 \right)$	(R6)	$\tilde{L}_{filter} = R_s \left(\hat{i}_{sd}^2 + \hat{i}_{sq}^2 \right)$	(R6e)

TABLE II.
POWER MODELING AND MANAGEMENT EQUATIONS

Modeling equations		Power management	
$p_{sto} = p_{bat} + p_{uc}$	(R7)	$p_{bat\_ref} = f(p_{sto\_ref})$ $p_{sc\_ref} = p_{sto\_ref} - \hat{p}_{bat}$	(R7c)
$p_{conv} = p_{pv} + p_{sto}$	(R8)	$p_{sto\_ref} = p_{conv\_ref} - \tilde{p}_{pv}$	(R8c)
$p_{AC} = p_{conv} - p_{DC}$	(R9)	$p_{conv\_ref} = p_{AC\_ref} + p_{DC\_ref}$	(R9c)
$p_g = p_{AC} - L_{filter}$	(R10)	$p_{AC\_ref} = p_{g\_ref} + \tilde{L}_{filter}$	(R10c)
$p_{DC} = u_{DC} \cdot i_{DC}$	(R11)	$p_{DC\_ref} = \hat{u}_{DC} \cdot i_{DC\_ref}$	(R11c)

By assuming a generating operation of batteries and supercapacitors and by neglecting losses in the power electronic converters, battery power p_{bat} and supercapacitor power p_{bat} appear directly to the DC-bus and are added to PV power p_{pv} (see Fig. 4 and Table II (R8)). A part of this power is exchanged inside DC-bus capacitor p_{DC} (see Table II (R9)). Some power is lost in choke L_{filter} and then the remaining power is sent to grid p_g (see Table II (R10)).

In this conversion chain studied, possibilities exist to store energy or to boost it by managing the exchanged power with batteries p_{bat} and with supercapacitors p_{sc} [25]. The management of the power flow is obtained by using the modelling equations in order to set the grid power with (p_{g_ref}) with prescribed DC-bus power (p_{dc_ref}) and under estimated available PV power $\tilde{p}_{pv}$. Losses in the grid filter can be estimated (see Table I (R6e)). They are used to calculate the AC power reference (p_{AC_ref}) (see Fig. 4 and Table II (R10c)).

In a similar, the power required to regulate DC-bus (p_{DC_ref}) is added to obtain the total power necessary (see Table II (R9c)). The reference of the exchanged power with the storage units (p_{sto_ref}) is calculated by using an estimation of PV power ($\tilde{p}_{pv}$) produced (see Table II (R8c)). Discharge of batteries is ordered from the grid power reference (Fig. 5). The loading of batteries is also ordered if excess power is available (p_{sto_ref} >0) and if an order from the grid power reference is received. The power reference of the supercapacitors is calculated from the difference between the timing reference of the required power from storage units p_{sto_ref} and calculated power reference of batteries ($\tilde{p}_{bat\_ref}$).

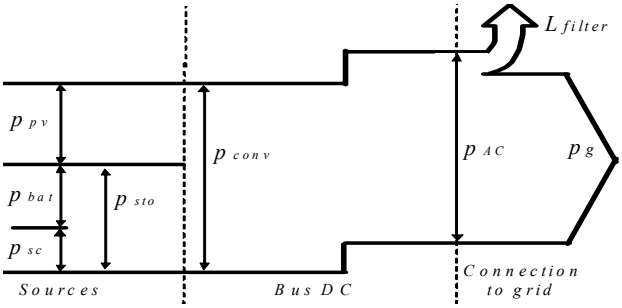

Fig. 3. Power flow for a generating mode of batteries and supercapacitors.

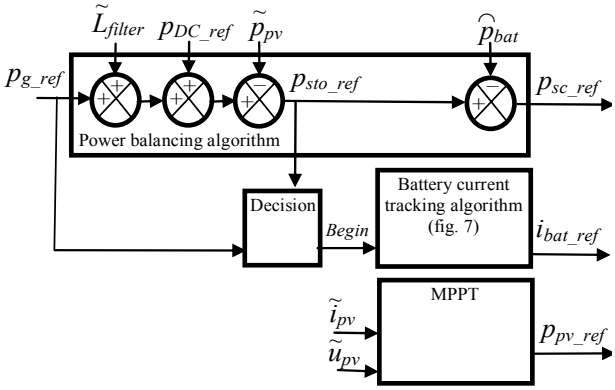

Fig. 4. Power algorithms.

III. BATTERY CURRENT TRACKING

A. Modeling of the lead acid battery

The availability of a theoretical charge voltage model, which is fitted to experimental data, is important to understand the behaviour of the batteries during charging in realistic conditions. Recently a fractional-order modelling has been developed to estimate the battery resistance [26]. Another method consists to use an extended Kalman filter for the observation battery parameters [27]. A charge voltage model can also be used to design the regulation system, the charge control and the global advanced PV control system with dedicated control functions for the grid. In this context, the most common models are electro-circuit models, which are based on electrical circuit elements such as capacitors, resistors, and a voltage source. Different electro-circuit

models for battery behaviour simulation are available, and these models have different degrees of complexity and simulation qualities.

However, among the models available, none is considered satisfactory in terms of complexity precision. The complexity is due to the high number of parameters to be determined. The major results show that for each battery, the parameter values are different and this is a major inconvenient for the regulation system design or PV general simulation. Therefore, it is preferable to have a generic model with constant parameters and valid for any size of batteries. In this context, in [28] a normalized model has been proposed. This model is simple because the experimental identification of empirical parameters is not required. The results, which have been obtained for different batteries in [28], [29] show that this model can adequately reproduce the behaviour of batteries during charge/discharge processes.

To avoid excessive complexity in this paper, a modified dynamical battery voltage model is proposed. It is based on the CIEMAT model [28]. A simple resistor-capacitor electrical model is used (see Fig. 5) and the terminal voltage is given as:

_ If $u_{bat}<nV_g$

$$u_{bat}(t)=n\left(V_{cb}(t)+V_{cp}(t)\right), \tag{1}$$

$$\begin{cases} \dfrac{dV_{cb}}{dt}=\dfrac{i_{bat}(t)}{C_b(t)} \\ \dfrac{dV_{cp}}{dt}=-\dfrac{1}{R(t)C_p}V_{cp}+\dfrac{i_{bat}(t)}{C_p} \end{cases} \tag{2}$$

$$SOC(t)=\frac{V_{cb}(t)-2}{0.16}. \tag{3}$$

_ If $u_{bat}\geq nV_g$

$$u_{bat}(t)=n\left(V_{cb}(t)+R(t)i_{bat}(t)\right), \tag{4}$$

$$SOC(t)=1, \tag{5}$$

$$V_{cb}(t)=2.16V \tag{6}$$

With

$$R(t)=\frac{1}{C_{10}}\left(\frac{6}{1+i_{bat}^{0.6}(t)}+\frac{0.48}{\left(1-\dfrac{(V_{cb}(t)-2)}{0.16}\right)^{1.2}}\right) \tag{7}$$

$$C_b(t)=\frac{1.67\,C_{10}}{1+0.67\left(\dfrac{i_{bat}(t)}{I_{10}}\right)^{0.9}}\frac{1}{n0.16}, \tag{8}$$

$$I_{10}=\frac{C_{10}}{10}. \tag{9}$$

i_{bat}: battery current (A), u_{bat}: battery voltage (V), n: number of cells, V_g=2.35V: gassing voltage, V_{cp}: polarization voltage (V), V_{cb}: electromotive force (V), *SOC*: battery state of charge, R: internal resistor, C_p: polarization capacitor (F), C_{10}: nominal capacity (Ah) after a 10h charging, I_{10}: charge current corresponding to C_{10}.

Model parameters have been identified for a battery pack, composed of four lead-acid STECO 3000 batteries. For each battery, the nominal capacity is C_{10}=95Ah, the nominal voltage is 12V and the number of cells is 6. In the battery pack, the serial/ parallel connection of four batteries is chosen to get a 24V full voltage with two sets in parallel of two batteries in series (see Fig. 2). Charge tests have been performed with a current–controlled DC/DC converter. During each test, the current and the temperature were kept constant. The polarization capacitance C_p=2000F obtained was been calculated to match with the test data. For a constant battery current (i_{bat}=5A), a comparison between the battery voltage and the model voltage is shown in Fig. 6.

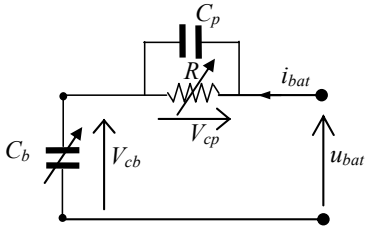

Fig. 5. Equivalent circuit for the battery.

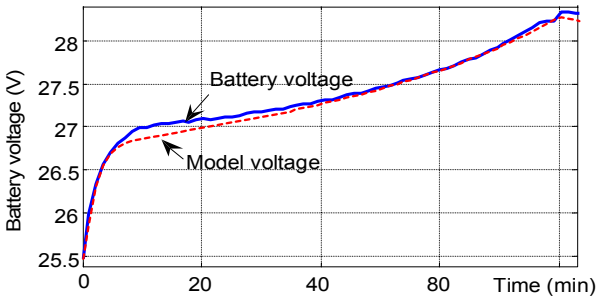

Fig. 6. Voltage-time characteristic with a 5A charge at 25°C.

B. Battery current tracking

The battery current tracking algorithm (see Fig. 4) is designed to determine the current and power references necessary to charge the battery. The estimation of the current and power reference is based on the battery model, which was proposed previously. Three remarks can be made:

- During the battery charging, if the battery current is maintained at a constant high level, the battery voltage increases fast until it reaches gassing voltage (V_g=2.35V). When the battery voltage exceeds this value, experimental results show that an excessive gas pressure in the battery may appear. The gas can escape through the safety valves, which reduces the battery lifetime and an explosion can occur.
- During the battery charging, the internal resistor still depends on battery *SOC*. Its value increases at a high rate when battery *SOC* is high. In this case, with a constant battery current, the battery losses are more important. Consequently, the battery efficiency is lower.
- If the battery is empty and with constant battery current $i_{bmax}=C_{10}/5$, *SOC* battery can only reach 68%. With constant battery current $i_{bmin}=C_{10}/100$, *SOC* battery can reach 95% but the charging time becomes longer than before.

In order to ensure a high *SOC* battery, a shorter time charging, an overcharge security and a high efficiency, it is important to reduce battery losses and to keep the battery voltage below the voltage gassing value. This can be expressed by the following conditions:

$$i_{bat\_ref}(t_0+\Delta t)R(t_0+\Delta t) \le i_{bat\_ref}(t_0)R(t_0) \quad \text{and} \quad u_{bat}(t_0) < nV_g \tag{10}$$

If these equations are summed, a single expression can be deduced:

$$i_{bat\_ref}(t_0+\Delta t) < \left[\frac{nV_g - u_{bat}(t_0) + i_{bat\_ref}(t_0)R(t_0)}{R(t_0+\Delta t)}\right] \tag{11}$$

Since the internal battery resistor has slow variations (Eq.(5)), this expression may be simplified:

$$i_{bat\_ref}(t_0+\Delta t) < \left[\frac{nV_g - u_{bat}(t_0)}{R(t_0)} + i_{bat\_ref}(t_0)\right] \tag{12}$$

According to equ. (4) when battery voltage u_{bat} reaches gazing voltage V_g, the internal battery resistor can be estimated from the following equation:

$$R(t_0) = \frac{V_g - 2.16}{i_{bat\_ref}(t_0)} \tag{13}$$

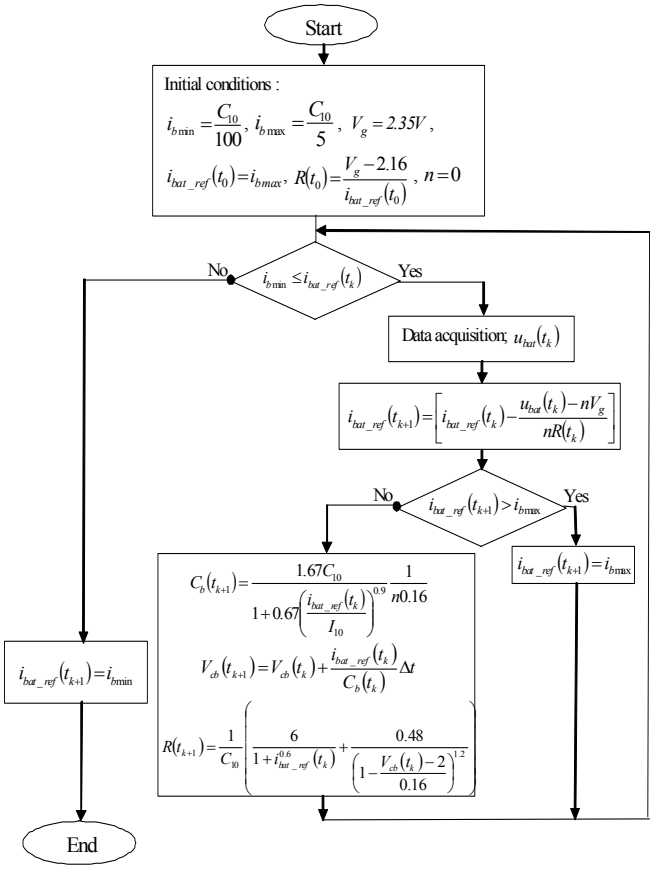

Fig. 7. Flowchart of the battery current tracking algorithm.

So the strategy used consists in loading the battery with a maximum current at the start and then to decrease it according to the proposed battery current tracking algorithm (see Fig. 7).

IV. Simulation Results

To verify the control scheme proposed, simulations of the control strategy of the lead-acid battery charger are first performed by using Matlab-Simulink software. The initial battery voltage is 25V.

For different initial battery currents i_{bmax} (10A and 20A), Fig. 8 and Fig. 9 show the calculated battery current reference by using the proposed method. The battery voltage obtained does not exceed the gassing voltage and the overcharge limit. For both tests, the battery voltage reaches the voltage value corresponding to the highest *SOC* battery level. The method proposed makes it possible to charge the battery in two stages: A "Bulk" phase is followed by an "Absorption" phase. During the "Bulk" phase, the battery voltage increases as the *SOC* increases. In this case, the calculated reference current depends on initial battery current i_{bmax}.

During the "Absorption" phase, the calculated battery current must be limited so that the charging voltage is maintained at a relatively high level to finish the charging of the battery within suitable time.

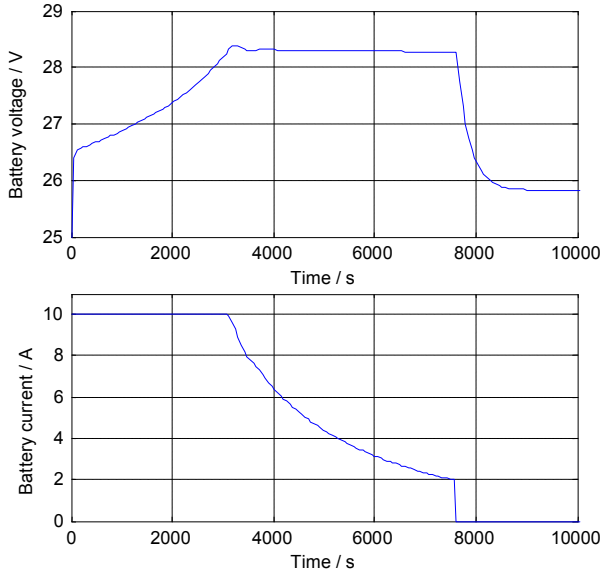

Fig. 8. Battery-charging process with initial battery current i_{bmax}=10A.

V. Experimental Validations

A. Test bench experimental results

A prototype has been built with six commercial half-bridge IGBT modules of two IGBT with diodes in parallel. All modules are in parallel on a common 48V DC bus (see Fig. 10). Although a Boost converter is sufficient to interface the two silicon nitride multicrystalline silicon PV modules used (BP3160, 24V-160W), an IGBT module is used to facilitate the mechanical design and maintenance.

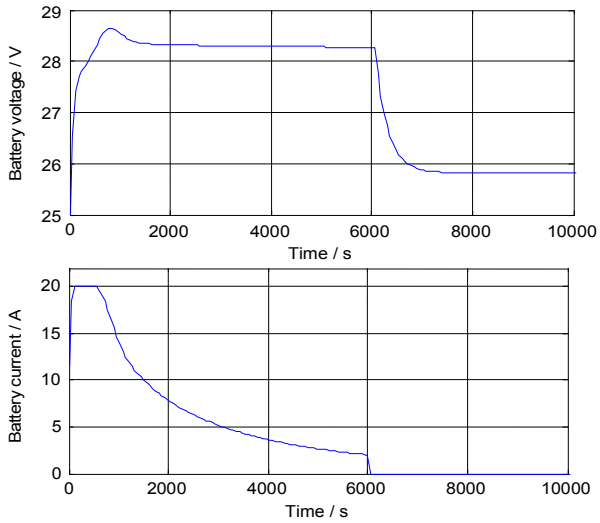

Fig. 9. Battery-charging process with initial battery current i_{bmax}=20A.

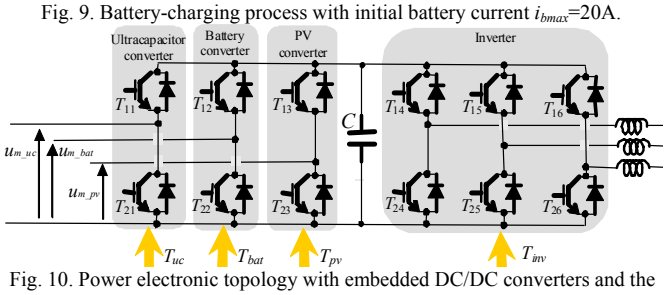

Fig. 10. Power electronic topology with embedded DC/DC converters and the inverter.

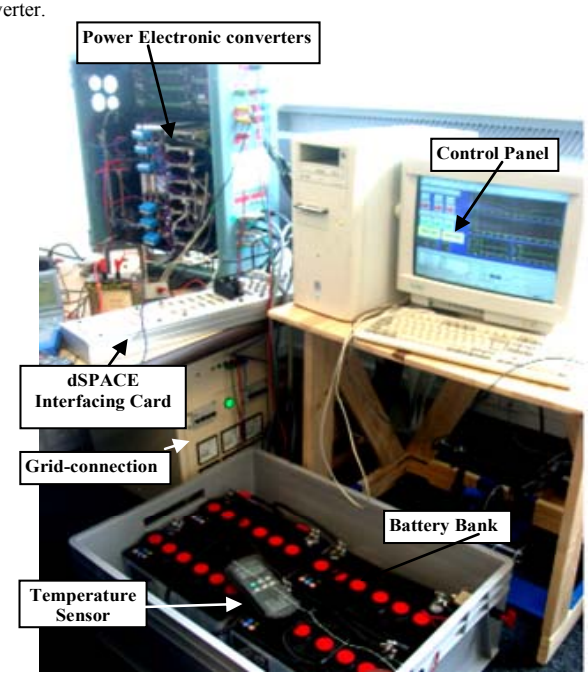

Fig. 11. Implementation of the experimental test bench.

Other implementations may be also considered as an example with a SEPIC converter [30].

One Boostcap super-capacitors module (160F-48V, BMOD2600-48EA) is used. The measurements of the battery current i_{bat} and the battery voltage u_{bat} are sensed with zero-flux hall-effect sensors. The proposed battery current tracking algorithm within the entire control system has been implemented on a real time card DSpace DS1103 (see Fig. 11), through the mathematical environment of Matlab-Simulink, with a 5kHz modulation frequency (for the SCU in Fig. 2), a 10kHz sampling frequency (for the ACU in Fig. 2) and with 0.5s for the time response of the PCU. The ControlDesk software enables changes in the parameters of the control system. Other system parameters are listed in Table III.

For the presented experimental results, the initial battery voltage is 25.46V. As there are 12 cells the initial cell voltage is then equal to 2.122V. The initial SOC battery was calculated by using (1) and (2) and it is equal to 76.09%. In order to verify the proposed control scheme, the maximum reference current is set to i_{bmax}=4,9A.

During the "Bulk" phase, the battery current remains constant and the battery voltage increases until it reaches the gassing voltage (see Fig. 12). During the "Absorption" phase, when the battery voltage is equal to the gassing voltage, the battery current is progressively reduced to 2A. At the end of this phase, the battery is left in open-circuit condition and the battery voltage, which is measured after 10h, is equal to 25.799V corresponding to 2.1499V for one battery cell. Therefore, the SOC battery is 93.7%. It was calculated by using (1) and (2).

A comparison between simulation and experimental results proves the success of the method proposed (see Fig. 13).

B. Applications for load following services

Power balancing between generators and loads is the most critical task in isolated networks since available generators designed for grid regulations (rms voltage and frequency for example) are limited [31].

TABLE III
PARAMETERS

L_1	3 mH	R_1	100mΩ
C_1	9.4μF	C	4.7 mF
L_2, L_3, L_4	10 mH	R_2, R_3, R_4	500mΩ

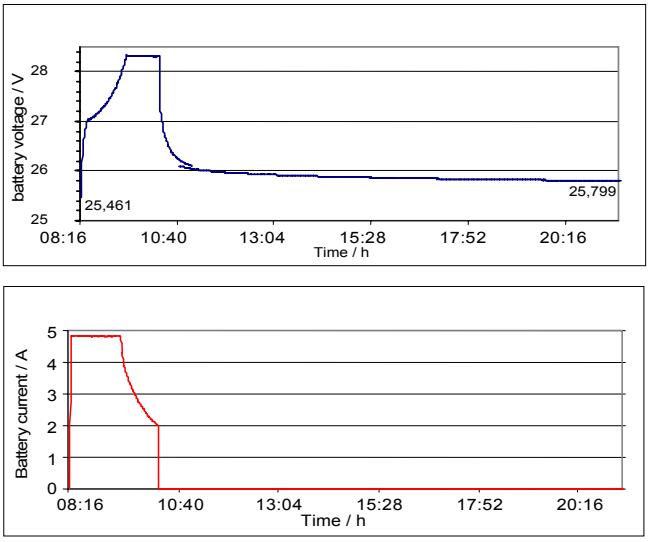

Fig. 12. Battery-charging process with initial battery current i_{bmax}=4.9A.

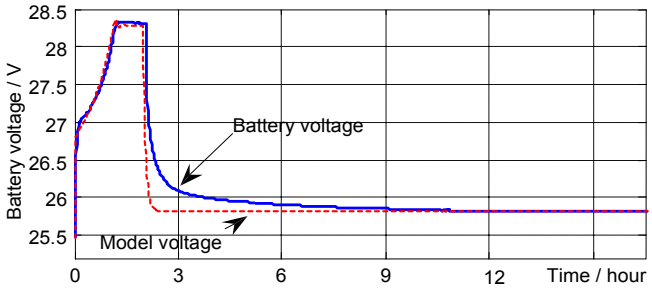

(a) battery current

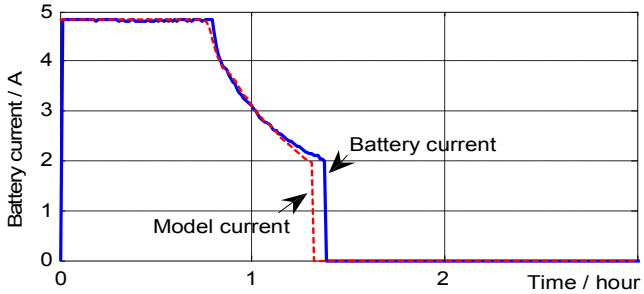

(b) battery current (zoomed view)

Fig. 13. Comparison between simulation and experimental results.

The "load following service" is implemented in a Central Microgrid Management System (CMMS) by the grid system operator [32]. He adjusts the power output of the generators dispatched (diesel groups, gas turbines …) according to daily electricity demand fluctuations. Embedded batteries in the hybrid active PV based DG studied gives an energy margin for the implementation of this service. So, this PV generator can now be interfaced with the CMMS and be used for "Load following services" as other dispatched generators. The DG considered is now planned and dispatched centrally in order to combine the response of classical generators and DG with on-demand load curtailments [33], [34]. This new distribution system is known as Microgrid and is very different from the existing distribution system. In this context, microgrid management and operation strategies give the higher priority to the use of renewable and sustainable DG. So, the PV based generator supplies the grid with prescribed power reference p_{g_ref}. As the demand significantly varies in the day (and also in the time of day during the week and year) the CMMS sends power set points for the real and reactive powers to the DG (see Fig. 14).

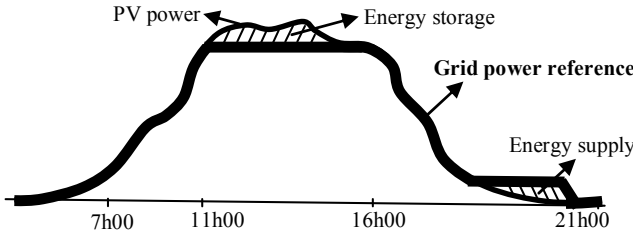

Fig. 14. Grid power reference for load following

C. Test of the grid following operation

As shown in Fig. 15, all the power produced from PV panels (signal 1) is generated to the grid before 19h00. Between 19h00 and 22h45, the micro grid operator sends a signal for an additional 2kW power for load following (signal 2), the reactive power reference is null in the results presented. The power requirement is quite well satisfied with an acceptable short time delay. The energy mainly comes from the batteries (see Fig. 16, blue signal 2) since the PV production continuously decreases (see Fig. 16, signal 1 in dashed lines). At steady state, the extracted power is more than 3kW, probably because of the filter losses compensation. Supercapacitors are requested for power supply in transient states at 19h00 and 22h45 (see Fig. 16, red signal 3 in dotted lines). As a result, the power of this hybrid active PV based generator generated follows the variations of the reference power, which is sent by the CMMS. This power reference comes from a "load following application", which also uses the other generators dispatched.

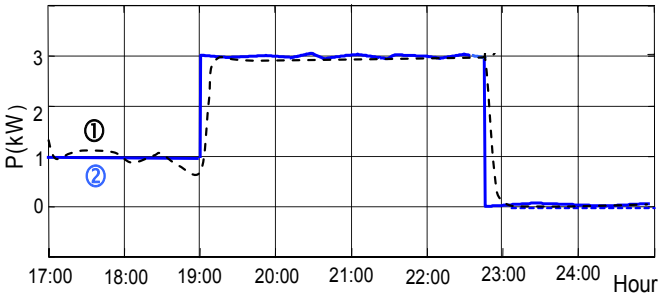

Fig. 15. Grid power p_g (signal 1) and requested power from the microgrid operator p_{gref} (signal 2).

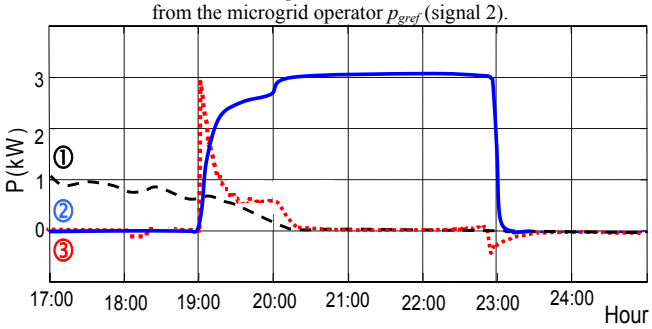

Fig. 16. Power from the sources, PV power p_{PV} (signal 1), battery power p_{bat} (signal 2), supercapacitor power p_{uc} (signal 3).

VI. Conclusion

Classical "renewable energy source-based systems" are passive generators, as they produce maximal (non-dispatched) power even though this power is not useful for the grid. In this paper, a PV-based hybrid active generator including lead-acid batteries and supercapacitors in a DC-coupled structure has been presented in order to deliver a prescribed power reference to the grid. The control system and the power management of the entire generator have been detailed. A special attention has been paid on the optimal battery charge. A specific algorithm for charge operating mode of lead-acid batteries has been proposed. The control design of charging the lead acid batteries has been developed and experimentally proved. Using the method proposed, the batteries can charge until a high SOC battery level and with overcharge security. Finally, the performances of this active generator for a load following application show that excessive or insufficient power from PV panels are well balanced by the two embedded storage units.

REFERENCES

[1] P.G. Barbosa, L.G.B. Rolim, E.H. Watanabe, R. Hanitsch, "Control strategy for grid-connected DC-AC converters with load power factor correction, Generation", *Proc. IEE Transmission and Distribution*, Vol. 145, Issue 5, pp. 487 – 491, Sep 1998.

[2] H. Yu, J. Pan, A. Xiang, "A multi-function grid-connected PV system with reactive power compensation for the grid", *Solar Energy*, vol. 79, iss. 1, pp. 101-106, July 2005.

[3] G. Delille, B. François, A review of some technical and economic features of energy storage technologies for distribution system integration, *Ecological engineering and environment protection*, pp. 40-48, vol. 1, ISSN 1311 – 8668, 2009.

[4] O. Gabriel, C. Saudemont, B. Robyns, M. Radulescu, "Control and performance evaluation of a flywheel energy-storage system associated to a variable-speed wind generator", *IEEE Trans. on Ind. Electron.*, Vol. 53, n° 4, pp. 1074-1085, 2006.

[5] S.J. Chiang, K.T. Chang, C.Y. Yen, "Residential photovoltaic energy storage system", *IEEE Trans. on Ind. Electron.*, vol. 45, iss. 3, pp385 – 394, June 1998.

[6] C.V. Nayar, M. Ashari, W.W.L. Keerthipala, "A grid-interactive photovoltaic uninterruptible power supply system using battery storage and a back up diesel generator", *IEEE Trans. on Energy Conversion*, Volume 15, iss. 3, pp. 348 – 353, Sep 2000.

[7] D. Lu, H. Fakham, T. Zhou, B. François, "Application of Petri Nets for the energy management of a photovoltaic based power station including storage units", *Renewable energy, Elsevier,* Volume 35, Issue 6, pp. 1117-1124 , 2010

[8] Y. K. Lo, H. J. Chiu, T. P. Lee, I. Purnama, J. M. Wang, "Analysis and Design of a Photovoltaic System DC connected to the Utility With a Power Factor Corrector", *IEEE Trans. on Ind. Electron.*, vol.56, iss. 11, pp. 4354- 4362, Nov. 2009

[9] P. Thounthong, S. Rael, B. Davat, "Control Strategy of Fuel Cell and Supercapacitors Association for a Distributed Generation System", *IEEE Trans. on Ind. Electron.*, vol.54, iss.6, pp. 3225–3233, Dec. 2007.

[10] C. Abbey and G. Joos, "Supercapacitor Energy Storage for Wind Energy Applications", *IEEE Trans. on Ind. Electron.*, vol.43, iss.3, pp.769-776, May 2007.

[11] H. Fakham, P. Degobert, B. François, "Control system and a power management for a PV based generation unit including storage units", *ACEMP'07 Electromotion'07,* Bodrum Turkey, 141-146, 2007.

[12] T. Yamazaki, K.-I. Muramoto, "An advanced solar charging and battery discharge controller unit", *Renewable Energy,* Volume 15, Number 1, pp. 606-609, September 1998.

[13] J.P. Dunlop, "Batteries and charge control in stand-alone photovoltaic systems, Fundamentals and application", Report prepared for Sandia National Laboratories, Florida Solar Energy Center, Jan.1997.

[14] S. Harrington, K. Corporation, J. Dunlop, "Battery Charge Controller Characteristics in Photovoltaic Systems", *IEEE AES Magazine,* Volume 7, Issue 8, pp.15 – 21, Aug. 1992.

[15] J. Woodworth, M. Thomas, J. Stevens, S. Harrington, J. Dunlop, M. Swamy, D. Leighton, "Evaluation of the batteries and charge controllers in small stand-alone photovoltaic systems", *24th IEEE Photovoltaic Specialists Conf., Hawaii,* USA, pp. 933–945, 1994.

[16] M. Fernandez, A.J. Ruddell, N. Vast, J. Esteban, F. Estela, "Development of a VRLA battery with improved separators and a charge controller for low cost photovoltaic and wind powered installations", *Journal of Power Sources*, 95, pp. 135–140, 2001.

[17] H. Masheleni, X.F. Carelse, "Microcontroller-based charge controller for stand-alone photovoltaic systems", *Solar Energy*, Volume 61, Number 4, pp. 225-230(6) , October 1998.

[18] O. Barbarisi, F. Vasca, L. Glielmo, "State of charge Kalman filter estimator for automotive batteries", *Control Engineering Practice*, 14, pp. 267-275, 2006.

[19] J. Wang, B. Cao, Q. Chen, "Combined state of charge estimator for electric vehicle battery pack", *Control Engineering Practice*, 15 (2007) 1569-1576.

[20] E. Koutrolis, K. Kalaitzakis, "Novel battery charging regulation system for photovoltaic applications", *IEE Proc. Electric Power Applications*, vol. 151, pp. 191-197, 2004.

[21] A. Daoud, A. Midoun, "Fuzzy Control of a Lead Acid Battery Charger", *Journal of Electrical Systems*, 1 (2005), pp. 52-59.

[22] B. Francois, J.P. Hautier, "Hierarchical control design using structural decomposition of a rectifier converter model", *Electrimacs'96,* Saint Nazaire, France, vol. 1, pp. 255-260, Sep. 1996.

[23] W. Xiao, P.R. Palmer, A. Capel, "Regulation of Photovoltaic voltage", *IEEE Trans. on Ind. Electron.*, Vol.54, iss.3, June 2007

[24] C. Hua, J. Lin, and Shen, "Implementation of dsp controlled photovoltaic system with peak power tracking", *IEEE Trans. on Ind. Electron.*, vol.45, iss. 1, pp. 99-107, Feb. 1998

[25] C. Meza, J. J. Negroni, D. Biel, F. Guinjoan, "Energy-Balance Modeling and Discrete Control for Single-Phase Grid-Connected PV Central Inverters", *IEEE Trans. on Ind. Electron.*, vol.55, iss. 7, pp. 2734-2743, Jul. 2008

[26] M. Cugnet, J. Sabatier, S. Laruelle, S. Grugeon, B. Sahut, A. Oustaloup, "On Lead-Acid-Battery Resistance and Cranking-Capability Estimation", *IEEE Trans. on Ind. Electron.*, vol.57, iss. 3, pp. 909-917, March 2010

[27] D.V. Do, C. Forgez, K. El Kadri Benkara, G. Friedrich, "Impedance Observer for a Li-ion Battery Using Kalman Filter", *IEEE Trans. on Vehicular Technology,* vol.58, No. 8, pp. 3930-3937, Oct. 2009

[28] J.B. Copetti, F. Chenlo, "A general battery model for PV system simulation", *Journal of Power Sources,* vol. 47, pp.109-118, 1994.

[29] D. Guasch, S. Silvestre, "Dynamic Battery Model for Photovoltaic Applications", *Progress in Photovoltaics, Research and Applications*, Volume 11 Issue 3, pp 193–206, Jan. 2003.

[30] C. Clastres T.T. Ha Pham, F. Wurtz, S. Bacha, "Ancillary services and optimal household energy management with PV production", *Energy*, Elsevier, Vol. 35, Iss. 1, pp. 55-64, Jan. 2010

[31] S.J. Chiang, H.J. Shieh, M.C. Chen, "Modeling and Control of PV charger With SEPIC Converter", *IEEE Trans. on Ind. Electron..*, vol.56, iss. 1, pp. 4344-4353, Nov. 2009

[32] D. Lu and B. Francois, "Strategic framework of an energy management of a microgrid with a photovoltaic-based active generator", *Electromotion'09*, 1-3, July, 2009, Lille, France.

[33] E. De Tuglie, F. Torelli, "Load Following Control Schemes for Deregulated Energy Markets", *IEEE Transactions on Power Systems*, vol.21, iss. 11, pp. 1691 – 1698, Nov. 2006.

[34] P. Li, P. Degobert, B. Robyns and B. Francois, "Participation in the frequency regulation control of a resilient microgrid for a distribution network*", International Journal of Integrated Energy Systems*, vol. 1, no1, Jan. 2009.

Bruno Francois (M'96-SM'06) received the Ph.D. degree in electrical engineering from the University of Lille, France in 1996. He is Associate Professor at the department of Electrical Engineering of Ecole Centrale de Lille and he is also a member of Laboratory of Electrical Engineering and Power electronic (L2EP), Lille. He has a long experience in the design of control systems for power electronic converters and more exactly multi-phase and multilevel converters. He is currently working on advanced renewable energy based generators and energy management systems for future smart grids.

Di Lu was born in Jiangsu, China, in 1983. He received the M.S. degree in electrical engineering from the University of Lille, France, in 2007. He is currently working toward the Ph.D. degree in electrical engineering in Laboratory of Electrical Engineering and Power electronic (L2EP), Lille, Ecole Centrale de Lille, France. His main research includes energy management and energy storage in distributed power generation systems based on renewable energy sources.

Hicham FAKHAM received the Ph.D. degree from the University of Versailles, France in 2006. He joined the Laboratory of Electrical Engineering and Power electronic of Lille (L2EP) in 2006. Currently, his main research interests include intelligent system applications in power engineering, and multi-agent systems.